Proc. Natl. Acad. Sci. USA
Vol. 78, No. 2, pp. 976–980, February 1981
Botany

Mathematical analysis of the chemosmotic polar diffusion of auxin through plant tissues

(indoleacetic acid/polar transport of auxin/cellular polarity)

MARY HELEN M. GOLDSMITH*, TIMOTHY H. GOLDSMITH*, AND MONROE H. MARTIN†

*Department of Biology, Yale University, New Haven, Connecticut 06520; and †Institute for Physical Science and Technology, University of Maryland, College Park, Maryland 20742

Communicated by Kenneth V. Thimann, October 17, 1980

ABSTRACT **Equations have been developed to describe the diffusional movement of a weak acid such as the auxin indoleacetic acid through a long file of vacuolated cells, where cellular accumulation is driven by the pH gradients across the cell membranes. If the permeability to the auxin anion is greater at one end of the cell than at the other, diffusional movement takes the form of polar transport, which exhibits: a nearly constant velocity either for the front or for a pulse of radioactive auxin, the capacity to move auxin against an external gradient of concentration, and a polar ratio that increases exponentially with the length of the section. The determinants of velocity include both diffusion through the vacuole and permeation steps at the cell membranes. Except for the permeabilities of the membranes to the anion, values are now available for all of the physical parameters in the equations. With reasonable estimates of permeability coefficients for the anion, the equations predict a velocity of transport of about 1 cm hr^{-1}, which agrees well with measured values. The analysis indicates, however, that the underlying cellular polarity may be greater than has been heretofore assumed. We thus demonstrate that the hypothesis of chemosmotic polar diffusion is capable of accounting quantitatively for the major features of auxin transport and provides a theoretical framework whose elements can be tested in future experiments.**

Since the early quantitative descriptions of the transport of the endogenous plant growth hormone auxin* (1–3) its cellular basis has been elusive. Among its characteristics are (*i*) a *polarity*, in which auxin moves more effectively through tissues in one direction than in the other, with the polar ratio increasing approximately exponentially with distance (4–6); (*ii*) the ability to move auxin through a tissue *against an external concentration gradient* (3); and (*iii*) a *velocity*, evidenced by a nearly constant rate of travel of 10 or more mm hr^{-1} of either the front (2, 4, 7–10) or a pulse of radioactively labeled auxin introduced at the apical end of a section (11). Various models involving differential secretion from the basal ends of the cells can account for the first two of these features, but there has been no convincing explanation for the third.

The *chemosmotic polar diffusion hypothesis* draws ideas and observations from several sources and postulates that polar transport involves both steps of membrane permeation and diffusion through the cell (12). Uptake of auxin is pH dependent and appears to be driven by the pH difference between the inside of the cell and the acidic wall space. With a difference of 2 pH units, and with only the undissociated acid permeant, auxin can accumulate passively to an internal concentration more than 50 times greater than the external. If the auxin anion is also permeant, this accumulation will be reduced. The suggestion that the polarity of transport is caused by a greater permeability to the anion at the basal than at the apical end of each cell (13, 14) is a central feature of this hypothesis.

Because neither cytoplasmic streaming (15) nor a lateral sheath of cytoplasm around the vacuole (16) is necessary to support transport, the auxin seems to cross the tonoplast and diffuse through the vacuole in traversing the length of each cell. The proposed path of auxin movement (Fig. 1) is as follows (12). Auxin permeates the apical plasmalemma, driven in by the metabolically maintained pH gradient. Because the cytoplasmic layer and the wall space are only about 1 μm thick, their concentrations of auxin can be considered spatially uniform at any time. A second permeation step occurs at the vacuolar membrane, followed by diffusion the length of the vacuole. Because the vacuole occupies most of the cross-sectional area of these cylindrical cells, and because centrifugation of the cytoplasm to the basal end does not slow transport (16), diffusional flux down the thin ensheathing layers of cytoplasm is ignored in this analysis. Exit from the cell is the reverse of entry, the only difference being a greater efflux of anion at the basal plasma membrane than at the apical. The process is repeated in subsequent cells in the file.

A formal mathematical description of this process would allow us to see whether reasonable values of permeability coefficients, diffusion constant, and pH gradient are consistent with the measured values of polarity and velocity of auxin transport. This formidable mathematical problem has recently been solved in a form applicable to nonelectrolytes (17). The purposes of this paper are to extend this analysis to weak acids and to compare quantitative predictions of the mathematical model with observations of auxin transport. By adjusting only the value of anion permeability, the model predicts the three properties of auxin transport: polarity, velocity, and the accumulation of auxin against an external gradient of concentration. Although our approach differs, our conclusions are similar to those of Mitchison (18).

RESULTS

Modification of Martin's equations for diffusional movement of a weak acid

In Martin's (17) treatment, the mass flux $\dot{M}$ of substance per unit area across one of the membranes is assumed to be proportional to the difference in concentration C on the two sides of the boundary. Thus

$$\dot{M} = \alpha_j(C_j - C_{j+1}),$$

in which α_j is a constant of proportionality, the permeability, and the subscripts designate the compartments on either side of the membrane. Auxin, however, exists as both the undissociated weak acid and the anion; consequently

The publication costs of this article were defrayed in part by page charge payment. This article must therefore be hereby marked "*advertisement*" in accordance with 18 U. S. C. §1734 solely to indicate this fact.

* Throughout this paper we use the generic term "auxin" to refer to the endogenous hormone indoleacetic acid, but the mathematical analysis applies to any acidic auxin that is polarly transported.

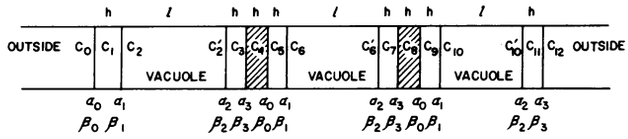

FIG. 1. Schematic drawing of tissue. The tissue section is considered to be a linear array of n cells, of which only three are shown. Hatched areas represent the walls, flanked by cytoplasmic layers, both of thickness h. Length of the vacuole is $l >> h$. α_0, β_0, α_3, and β_3 relate to fluxes at the plasmalemma; α_1, β_1, α_2, and β_2, fluxes at the tonoplast, and are defined in the text. Notation follows ref. 17 and *Appendix*.

$$C = HA + A^-.$$

Studies of uptake of auxin indicate permeability to the anion as well as the acid, and provide some evidence for a proton symport (19–21). The effect of such a symport is to remove the voltage dependence from a fraction of the anion permeability P'_{A^-}. Therefore an expression for the mass flux is

$$\dot{M} = P_{HA}(HA_j - HA_{j+1}) + P_{A^-}\left(\frac{\phi}{e^{\phi} - 1}\right)(A_j^- - e^{\phi}A_{j+1}^-) + P'_{A^-}(A_j^- - A_{j+1}^-), \quad [1]$$

in which ϕ is zVF/RT, an electrical term encompassing the effect of membrane voltage on the flux of anions, R is the gas constant, T the absolute temperature, z the valence (-1), F the Faraday constant, and V the membrane voltage ($V_{j+1} - V_j$).

In each compartment the concentrations A^-, HA, and H^+ are related by the dissociation constant K_a:

$$K_a = H^+ \cdot A^-/HA.$$

Therefore $HA_j = C_j/(1 + 10^{pH_j - pK})$ and $A_j^- = C_j 10^{pH_j - pK}/(1 + 10^{pH_j - pK})$, in which pH and pK have their usual meanings; i.e., $pH = -\log H^+$ and $pK = -\log K_a$. Substituting these expressions for concentration into Eq. 1 and rearranging, the equation for mass flux takes the form

$$\dot{M} = \alpha_j C_j - \beta_j C_{j+1}, \quad [2]$$

in which

$$\alpha_j = \frac{P_{HA} + \left[P_{A^-}\left(\frac{\phi}{e^{\phi} - 1}\right) + P'_{A^-}\right]10^{pH_j - pK}}{1 + 10^{pH_j - pK}} \quad [3a]$$

$$\beta_j = \frac{P_{HA} + \left[P_{A^-}\left(\frac{\phi e^{\phi}}{e^{\phi} - 1}\right) + P'_{A^-}\right]10^{pH_{j+1} - pK}}{1 + 10^{pH_{j+1} - pK}}. \quad [3b]$$

In general, with $pH_j \neq pH_{j+1}$ and $V \neq 0$, then $\alpha_j \neq \beta_j$. The previously published mathematical treatment of diffusional movement through a series of membranes and vacuoles (17) assumes $\alpha_j = \beta_j$; *Theorems 8.1* and *8.1'* in *Appendix* of this paper set forth the necessary modifications for the biologically more interesting case in which $\alpha_j \neq \beta_j$.

The physical interpretation of P_{HA} is straightforward: the permeability coefficient for the undissociated acid. The physical interpretation of P_{A^-} and P'_{A^-}, on the other hand, is less obvious. There is evidence that one or more carriers are involved in the transmembrane fluxes of A^- (13, 19–21), and under these circumstances the expressions for α_j and β_j are approximately correct only if the concentrations of A^- are assumed to be well below carrier saturation. Because auxin has its physiological effects in the micromolar range, this assumption is reasonable.

If the carrier concentrations remain the same on the two sides of the membrane, P_{A^-} (or P'_{A^-}) = $P_{XA}X/K_d$, in which P_{XA} is the permeability of the loaded carrier, X is the carrier concentration, and K_d is the dissociation constant for the reaction $A^- + X \rightleftarrows AX^-$. If, on the other hand, the carrier redistributes across the membrane in response to the concentration gradient of A^-, X_j becomes a nonlinear function of A_j^- and the terms in Eq. 1 that represent the fluxes of anion are only approximations.

Predictions of the equations for auxin transport

Using a computer, we obtained numerical results (*Theorems 8.1* and *8.1'*, *Appendix*) for the wall concentration relative to the donor concentration (W_m/C_0) as a function of both distance into the section (cell number, m) and time. The concentration at the "receiving end" was held at zero for these calculations. Numerical values for all parameters for which independent estimates are available are as follows: indoleacetic acid diffusion coefficient $D = 7 \times 10^{-6}$ cm^2 sec^{-1} (22); permeability coefficient of the undissociated acid $P_{HA} = 3.3 \times 10^{-3}$ cm sec^{-1} (14, 23); membrane voltage at the plasmalemma $V = 100$ mV (unpublished observation); wall pH = 5 (24, 25); cytoplasmic pH = 7.2 (26); and vacuolar pH = 5.5 (ref. 26; unpublished observation). Vacuolar length l was taken as 100 μm, and cytoplasm and wall thickness $h = 1$ μm (*Theorem 8.1*) or $h = 0$ (*Theorem 8.1'*). The pK_a of indoleacetic acid is 4.7. The utility of the mathematical model is considerable, for although it is intended to describe a complex biological system, there remain only two related parameters for which there are no independent estimates. These are the values of P_{A^-} (or P'_{A^-}) at the apical and basal ends of the cell.

The family of unbroken sigmoid curves in Fig. 2 shows the distribution of auxin in the walls as a function of position in the section at 3-min intervals. For these solid curves, the permeability to the anion at the basal plasma membrane of each cell was assumed to be larger than at the apical end; this produces

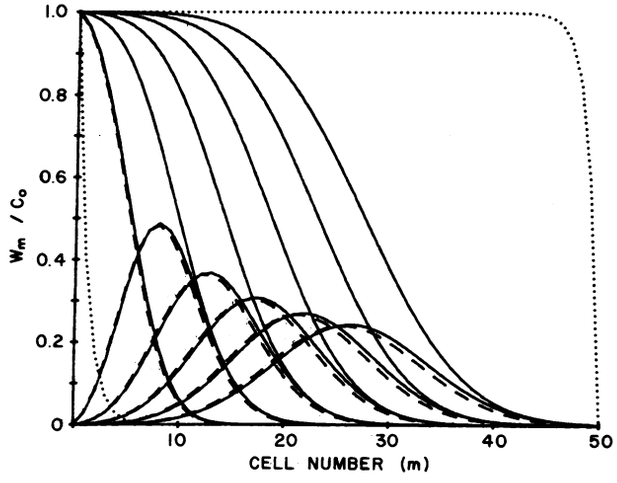

FIG. 2. Distribution of auxin in walls as a function of distance and time. Unbroken sigmoid curves show the progressive basipetal movement of the front at 3-min intervals through a 5-mm section, calculated from *Theorem 8.1'* (*Appendix*). W_m/C_0 is the wall concentration in the mth cell, relative to the source. The other solid curves show the corresponding movement of a pulse when the source concentration is C_0 for 3 min and 0 thereafter. Dashed curves show the small slowing of the pulse when the cytoplasm and wall thickness is 1 μm (*Theorem 8.1*) rather than 0. Cellular polarity $\mu = 2.437$. Cellular polarity assumes this value with a symport present at all membranes ($P_{A^-} = 3.3 \times 10^{-3}$ cm sec^{-1}) and a voltage-sensitive anion leak at only the basal plasmalemma ($P_{A^-} = 1.24 \times 10^{-3}$ cm sec^{-1}). The dotted curves show the steady-state concentrations; the one on the left is for acropetal movement through the same file of cells—i.e., cellular polarity = 1/2.437.

basipetal transport of auxin. The dotted curves show the steady-state distributions of auxin for basipetal (right) and acropetal (left) transport, for the boundary conditions $W_0 = C_0$, $W_n = 0$. Clearly the assumption of different anion permeabilities at the two ends of each cell leads to an asymmetry of auxin movement through the tissue.

Movement of a Pulse; Velocity of Transport. After application of radioactive auxin to the apical end of a tissue section for several minutes, a peak of labeled auxin moves through the tissue at about 10 mm hr^{-1}. As it moves, the spatial distribution of label becomes less compact, and the amplitude of the peak decreases (11).

The mathematical analysis predicts such a basipetally moving pulse (Fig. 2). Velocity can be calculated from the movement of the peak of the pulse or from the movement of the center of mass ($\Sigma mW_m/\Sigma W_m$), and in this example is about 9 mm hr^{-1}. The model therefore predicts a second characteristic of auxin transport, a nearly constant velocity.

Effect of h, Cytoplasm, and Wall Thickness. If $h = 0$, *Theorem 8.1* simplifies to *8.1'*. The difference between the unbroken curves in Fig. 2 ($h = 0$) and the dashed curves ($h = 1$ μm) is inconsequential, and most of the computations reported in this paper therefore assumed $h = 0$ and employed *Theorem 8.1'*.

Cellular Polarity, μ. The parameter μ in *Theorem 8.1* provides a measure of the cellular polarity that underlies this asymmetric diffusion. The parameter μ (*Appendix*) is defined in terms of the coefficients α and β (see Fig. 1); i.e.,

$$\mu = \alpha_0\alpha_1\alpha_2\alpha_3/\beta_0\beta_1\beta_2\beta_3 = \alpha/\beta. \quad [4]$$

If the tonoplast membrane is identical at the two ends of the vacuole, $\alpha_1 = \beta_2$, $\alpha_2 = \beta_1$, and

$$\mu = \alpha_0\alpha_3/\beta_0\beta_3 = \alpha/\beta.$$

The physical significance of μ is as follows. If the concentration of auxin at the apical end of a cell were held at C_0 while auxin diffused through the cell into a small extracellular reservoir at the base, diffusional equilibrium would be reached when the concentration W in the basal wall had risen to $C_0\mu$. For a file n cells in length, diffusional equilibrium would therefore be reached when the concentration at the basal end of the nth cell was $W_n = C_0\mu^n$. For basipetal transport, cellular polarity is μ and $\mu > 1$; for acropetal transport, cellular polarity is $1/\mu$. For $\mu > 1$, basipetal transport can proceed against a gradient as long as $W_n < C_0\mu^n$. The model therefore accounts for transport against an external gradient of concentration.

Polar Ratio in Transporting Sections. Although transport to equilibrium has not been measured in living tissue, we can compare some experimental data on polarity with theory in the following way. The polar ratio has been operationally defined (5) as the amount of auxin that has passed through a plane at distance d from an apical source after a period of basipetal transport t, divided by the amount of auxin that has passed through a plane at distance d from a basal source after t min of acropetal transport. This ratio increases exponentially with d (5).

In a completely analogous fashion, the polar ratio can be predicted from the theoretical curves by

$$R = \sum_{m=d}^{n} W_m^b \Big/ \sum_{m=d}^{n} W_m^a,$$

in which W^b and W^a represent wall concentrations for basipetal and acropetal transport, respectively, and distance is measured by number of cells m. Note that *Theorems 8.1* and *8.1'* require that W_n = a constant, which is accomplished in both theory and experiment by making the column of cells long enough that the concentration at the distal end does not rise appreciably above 0 in time t. In Fig. 3, μ was altered by varying the wall pH. The theory clearly predicts that polar ratio increases exponentially with distance transported.

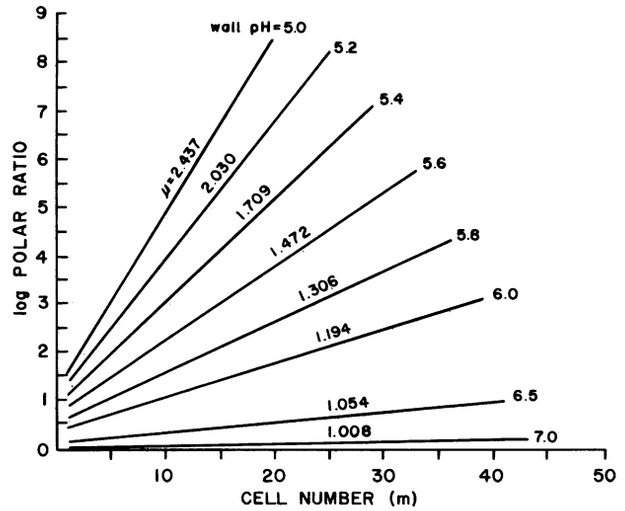

FIG. 3. Calculated logarithm of polar ratio of transport (see text for definition) as a function of length of section, for several values of μ. Cellular polarity μ was adjusted by altering the external (cell wall) pH, as indicated. Polar ratio increases exponentially with length of section.

What Determines Velocity of Transport? Velocity depends on two factors: (*i*) the resistance to movement at the membranes and in the vacuole, as measured by the permeability and diffusion coefficients, and (*ii*) the net driving force for auxin across the cell, as measured by μ. Diffusion coefficient and cell length influence only *i*, whereas the permeability coefficients contribute to both *i* and *ii*. If the tonoplast has identical properties at both ends, its permeability contributes only to *i*.

Fig. 4 shows the effect on velocity of varying the resistive parameters D, l, and the anion permeability of the tonoplast $P_{A^-}^{tnp}$. With the parameters used, the diffusional resistance of the vacuole is more important than the barrier presented by the tonoplast. Velocity should be higher in shorter cells, but it is not likely to be greatly influenced by the probable magnitude of any errors in the published measurment of D.

Important as these parameters are, the velocity (and polar ratio) can be more strongly dependent on μ. As the external

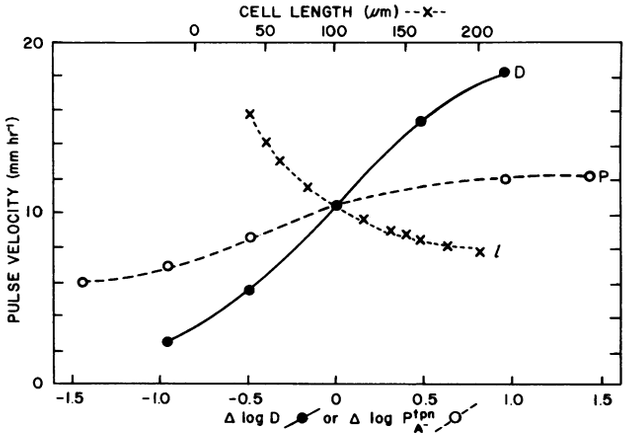

FIG. 4. Effect of changes in diffusion coefficient, cell length, and tonoplast permeability on velocity of transport under conditions of constant cellular polarity, $\mu = 2.437$. Parameters are similar to those in Fig. 2.

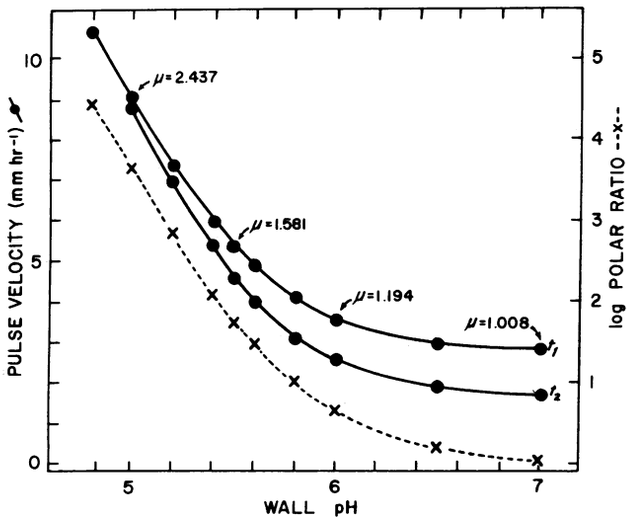

FIG. 5. Calculated pulse velocity (unbroken curves) and polar ratio per mm (dashed curve) as a function of wall pH. Changes in external pH alter the cellular polarity μ, as indicated in the figure, but the resistive terms (permeability and diffusion coefficients, cell length) remain unchanged. The lower plot of pulse velocity is for a time 9 min after the upper curve. Velocity therefore slows with time, but the change is relatively small with larger values of μ.

(wall) pH is allowed to rise from 5 to 7, the permeability terms in α and β remain constant, and μ (in the specific example under discussion) falls from 2.437 to 1.008. Fig. 5 shows the steep dependence of both velocity and polar ratio on wall pH, and thus on the cellular polarity μ. This analysis leads to the prediction that polarity of transport should be inhibited by buffering the wall space at a less acid pH than is normal, a prediction for which there is some evidence (unpublished observations).

DISCUSSION

Origin of μ. From the definition of μ (Eq. 4) and the dependence of α_j and β_j on the permeabilities (Eqs. 3a and 3b), it would seem that apical/basal differences in either the voltage-sensitive (P_{A^-}) or voltage-insensitive (P'_{A^-}) components of anion flux could contribute to cellular polarity. A realistic kinetic model for the voltage-insensitive permeation—as an anion–proton symport—indicates, however, that such a path would contribute to the transmembrane flux of auxin but would not constitute an anion "leak" that lowers the equilibrium uptake of auxin by the cell (ref. 19). This suggests that the origin of μ is a difference in the ratio $P_{A^-}/(P_{HA} + P'_{A^-})$ at the top and bottom of the cell, and that the presence of a symport enhances the membrane's permeability to auxin without collapsing the accumulation of auxin by the cell.

Magnitude of μ. The example of Fig. 2 predicts a velocity of transport at a wall pH = 5 that is similar to measured values, but the predicted polar ratios of $10^{3.4}$ mm^{-1} are considerably larger than the experimental values reported by de la Fuente and Leopold (5). This is a direct result of a cellular polarity of 2.4 rather than the 1.05–1.1 inferred by Leopold and Hall (6). The present analysis indicates that, in order to support a velocity of about 10 mm hr^{-1}, cellular polarity must be larger than heretofore supposed, and we suggest that with high values of μ the measured polar ratio is inevitably degraded by acropetal diffusion of auxin through the extracellular wall space. Measured values of polar ratio therefore may not provide an adequate way to estimate μ. The need for cellular polarities of at least 1.5 has been independently suggested by Mitchison (18).

Velocity is more nearly constant the higher the value of μ (Fig. 5). In the limiting case of $\mu = 1$, the front decelerates, as in simple diffusion. A sufficiently high value of μ is therefore necessary to account for the approximate constancy of velocity as well as its magnitude.

APPENDIX

We set forth in this appendix the modifications needed in key formulas and theorems of ref. 17 to treat the assumption that the mass flux $\dot{M}$ across a boundary is a linear combination of the concentrations on the two sides of the boundary, rather than simply proportional to the concentration difference. The numeration of ref. 17 is retained.

$$\dot{M} = \alpha_0 C_0 - \beta_0 C_1,\ \dot{M} = \alpha_1 C_1 - \beta_1 C_2,$$

$$\dot{M} = \alpha_2 C'_2 - \beta_2 C_3,\ \dot{M} = \alpha_3 C_3 - \beta_3 C_4, \text{ etc.} \quad [1.2]$$

$$DC_x = \beta_1 C_2 - \alpha_1 C_1,\ DC_x = \beta_2 C_3 - \alpha_2 C'_2, \text{ etc.} \quad [1.3]$$

$$c_4 = \bar{\kappa}(\alpha c_0 + \beta c_8),\ \alpha = \alpha_0\alpha_1\alpha_2\alpha_3,\ \beta = \beta_0\beta_1\beta_2\beta_3, \quad [5.4]$$

$$\bar{\kappa} = \Big[\sqrt{Ds}(\beta_0 + \alpha_1 + hs)(\beta_2 + \alpha_3 + hs)(\beta_3 + \alpha_0 + hs - \beta_0 a_1 - \alpha_3 b_3)A\Big]^{-1}.$$

$$\bar{\kappa} = \Big[P\cosh(k\sqrt{s}) + Q\sqrt{Ds}\sinh(k\sqrt{s})\Big]^{-1}. \quad [5.5]$$

$$P_0 = \alpha + \beta, \quad [5.6']$$

$$P_1 = \alpha_1\alpha_2\alpha_3 + \alpha_1\alpha_2\beta_3 + \beta_1\beta_2\beta_3 + \alpha_0\alpha_2\alpha_3 + \beta_0\alpha_2\alpha_3 + \beta_0\alpha_2\beta_3 + \alpha_0\beta_1\alpha_3 + \beta_0\beta_1\alpha_3 + \beta_0\beta_1\beta_3 + \alpha_0\alpha_1\alpha_2 + \alpha_0\beta_1\beta_2 + \beta_0\beta_1\beta_2,$$

$$P_2 = \alpha_0\beta_1 + \beta_0\beta_1 + \alpha_0\alpha_2 + \beta_0\alpha_2 + \alpha_1\alpha_2 + \beta_1\beta_2 + \beta_1\alpha_3 + \beta_1\beta_3 + \alpha_2\alpha_3 + \alpha_2\beta_3,$$

$$P_3 = \beta_1 + \alpha_2,$$

$$Q_0 = \alpha_1\beta_2\beta_3 + \beta_0\beta_2\beta_3 + \alpha_0\alpha_1\alpha_3 + \alpha_0\alpha_1\beta_2,$$

$$Q_1 = \alpha_0\alpha_1 + \alpha_0\beta_2 + \beta_0\beta_2 + \alpha_0\alpha_3 + \beta_0\alpha_3 + \beta_0\beta_3 + \alpha_1\beta_2 + \alpha_1\alpha_3 + \alpha_1\beta_3 + \beta_2\beta_3,$$

$$Q_2 = \alpha_0 + \beta_0 + \alpha_1 + \beta_2 + \alpha_3 + \beta_3,$$

$$R_0 = (\beta_1\alpha_2/D)(\alpha_0\alpha_3 + \beta_0\alpha_3 + \beta_0\beta_3),$$

$$R_1 = (\beta_1\alpha_2/D)(\alpha_0 + \beta_0 + \alpha_3 + \beta_3),$$

$$R_2 = \beta_1\alpha_2/D.$$

$$w_r = \bar{\kappa}(\alpha w_{r-1} + \beta w_{r+1}),\ r = 1,2,\ldots \quad [5.7]$$

$$B_0 = 1,\ B_1 = 1,\ B_2 = 1 - \lambda^2,$$

$$B_3 = 1 - 2\lambda^2,\ \lambda^2 = \alpha\beta\bar{\kappa}^2, \quad [5.11]$$

$$w_{n-1} = \alpha^{n-1}\frac{\bar{\kappa}^{n-1}}{B_{n-1}}w_0 + \beta\bar{\kappa}\frac{B_{n-2}}{B_{n-1}}w_n,\ n = 2, 3, 4. \quad [5.12]$$

$$\sqrt{\alpha\beta}/\lambda = P\cosh(k\sqrt{s}) + Q\sqrt{Ds}\sinh(k\sqrt{s}), \quad [7.1]$$

$$2\sqrt{\alpha\beta}\cos\theta = P\cosh(k\sqrt{s}) + Q\sqrt{Ds}\sinh(k\sqrt{s}). \quad [7.1']$$

$$F(h,s) = P\cosh(k\sqrt{s}) + Q\sqrt{Ds}\sinh(k\sqrt{s}) - 2\sqrt{\alpha\beta}\cos\theta_q = 0,\ q = 1, \ldots, n-1, \quad [7.2]$$

$$\sigma_0\cosh(k\sqrt{s}) + \sqrt{s}\sinh(k\sqrt{s}) - \sigma_1\cos\theta_q = 0,$$

$$\sigma_0 = P_0/\sqrt{D}Q_0,\ \sigma_1 = 2\sqrt{\alpha\beta}/\sqrt{D}Q_0. \quad [7.2']$$

In figure 2 of ref. 17 replace $y = \sigma_0\cos\theta_q$ by $y = \sigma_1\cos\theta_q$. Note that $\sigma_1 \leqq \sigma_0$.

$$Y(h,\eta_{qr}(h)) = \frac{k\sqrt{D}Q + 2P_s}{4\sqrt{\alpha\beta}}\cos k\eta_{qr}(h) + \frac{kP + \sqrt{D}Q - 2\sqrt{D}\eta_{qr}^2(h)Q_s}{4\sqrt{\alpha\beta}}\frac{\sin k\eta_{qr}(h)}{\eta_{qr}(h)}. \quad [7.13]$$

$$\rho(b_m;s_{qr}(h)) = \frac{(-1)^{q+1}}{n}\left(\frac{\beta}{\alpha}\right)^{(n-m)/2}\frac{\sin\theta_q\sin m\theta_q}{Y(h,\eta_{qr}(h))},$$

$$\rho(a_m;s_{qr}(h)) = \frac{(-1)^{q+1}}{n}\left(\frac{\alpha}{\beta}\right)^{m/2}\frac{\sin\theta_q\sin(n-m)\theta_q}{Y(h,\eta_{qr}(h))}. \quad [7.14]$$

$$W_m = C_0F_m + C_{4n}G_m, \quad [8.6]$$

$$G_m = \frac{\mu^m-1}{\mu^n-1} - \sum_{q=1}^{n-1}\sum_{r=0}^{\infty}\frac{\rho(b_m;s_{qr}(h))}{\eta_{qr}^2(h)}e^{-\eta_{qr}^2(h)t},$$

$$\mu = \frac{\alpha}{\beta},\ q \neq p\frac{\pi}{d},\ p = 0, \ldots, d, \quad [8.9]$$

$$F_m = \frac{\mu^n - \mu^m}{\mu^n - 1} - \sum_{q=1}^{n-1}\sum_{r=0}^{\infty}\frac{\rho(a_m;s_{qr}(h))}{\eta_{qr}^2(h)}e^{-\eta_{qr}^2(h)t}. \quad [8.9']$$

$$P\cos k\eta - \sqrt{D}\eta Q\sin k\eta - 2\sqrt{\alpha\beta}\cos\theta_q = 0,$$

$$\theta_q = q\frac{\pi}{n},\ q = 1, \ldots, n-1, \quad [8.11]$$

$$0 \leqq t,\ 0 \leqq h \leqq h_0. \quad [8.12]$$

THEOREM 8.1. *When the outside concentrations* C_0, C_{4n} *are constant, the concentration* W_m *in the* m*th wall is given by Eq. 8.6 in which the functions* F_m, G_m *of* t,h *defined in Eqs. 8.9 and 8.9′ are continuous functions of* t,h *in the interval 8.12. The residues* $\rho(a_m;s_{qr}(h))$, $\rho(b_m;s_{qr}(h))$ *in these expressions are defined in Eqs. 7.13 and 7.14, in which* $\eta_{qr}(h)$ *are the roots of 8.11.*

THEOREM 8.1′. *When* h = 0 *and the outside concentrations* C_0, C_{4n} *are constant, the concentration* W_m *in the* m*th wall is given by Eq. 8.6, in which*

$$F_m = \frac{\mu^n - \mu^m}{\mu^n - 1} + \frac{\mu^{m/2}}{n}\sum_{q=1}^{n-1}\sum_{r=0}^{\infty}(-1)^q\frac{\sin\theta_q\sin(n-m)\theta_q}{\eta_{qr}^2Y(\eta_{qr})}e^{-\eta_{qr}^2t},$$

$$\theta_q = q\frac{\pi}{n} \neq p\frac{\pi}{n},\ p = 0, \ldots, d,$$

$$G_m = \frac{\mu^m - 1}{\mu^n - 1} + \frac{\mu^{-(n-m)/2}}{n}\sum_{q=1}^{n-1}\sum_{r=0}^{\infty}(-1)^q\frac{\sin\theta_q\sin m\theta_q}{\eta_{qr}^2Y(\eta_{qr})}e^{-\eta_{qr}^2t},$$

$$\mu = \frac{\alpha}{\beta}$$

in which d *is the greatest common divisor of* m, n, *with*

$$Y(\eta_{qr}) = \frac{k}{2\sigma_1}\cos k\eta_{qr} + \frac{k\sigma_0 + 1}{2\sigma_1}\frac{\sin k\eta_{q_r}}{\eta_{qr}},$$

$$\sigma_0 = \frac{P_0}{\sqrt{D}Q_0},\quad \sigma_1 = \frac{2\sqrt{\alpha\beta}}{\sqrt{D}Q_0},$$

and η_{qr} *are the roots of*

$$\sigma_0\cos k\eta - \eta\sin k\eta - \sigma_1\cos\theta_q = 0$$

pictured in figure 2 of ref. 17.

In figure 4 of ref. 17 replace $\frac{n-m}{n}C_0$ by $\frac{\mu^n - \mu^m}{\mu^n - 1}C_0$ and $\frac{m}{n}C_{4n}$ by $\frac{\mu^m - 1}{\mu^n - 1}C_{4n}$.

This research was supported by grants from the National Science Foundation (PCM 78-10198) and the National Institutes of Health (EY00222).

1. Went, F. W. (1928) *Recl. Trav. Bot. Neerl.* **25,** 1–116.
2. van der Weij, H. G. (1932) *Recl. Trav. Bot. Neerl.* **29,** 380–496.
3. van der Weij, H. G. (1934) *Recl. Trav. Bot. Neerl.* **31,** 810–857.
4. Went, F. & White, R. (1939) *Bot. Gaz. (Chicago)* **100,** 465–484.
5. de la Fuente, R. K. & Leopold, A. C. (1966) *Plant Physiol.* **41,** 1481–1484.
6. Leopold, A. C. & Hall, O. F. (1966) *Plant Physiol.* **41,** 1476–1480.
7. Leopold, A. C. & Lam, S. L. (1961) in *Plant Growth Regulation,* ed. Klein, R. M. (Iowa State Univ., Ames, IA), pp. 411–418.
8. McCready, C. C. (1963) *New Phytol.* **62,** 3–18.
9. McCready, C. C. & Jacobs, W. P. (1963) *New Phytol.* **62,** 19–34.
10. Pilet, P. E. (1965) *Physiol. Plant.* **18,** 687–702.
11. Goldsmith, M. H. M. (1967) *Plant Physiol.* **42,** 258–263.
12. Goldsmith, M. H. M. (1977) *Annu. Rev. Plant Physiol.* **28,** 439–478.
13. Rubery, P. H. & Sheldrake, A. R. (1974) *Planta* **118,** 101–121.
14. Raven, J. A. (1975) *New Phytol.* **74,** 163–172.
15. Cande, W. Z., Goldsmith, M. H. M. & Ray, P. M. (1973) *Planta* **111,** 279–296.
16. Goldsmith, M. H. M. & Ray, P. M. (1973) *Planta* **111,** 297–314.
17. Martin, M. H. (1980) *Mathematical Modelling* **1,** 141–166.
18. Mitchison, G. J. (1980) *Proc. R. Soc. London Ser. B* **209,** 489–511.
19. Rubery, P. H. (1978) *Planta* **142,** 203–206.
20. Rubery, P. H. (1979) *Planta* **144,** 173–178.
21. Edwards, K. L. & Goldsmith, M. H. M. (1980) *Planta* **147,** 457–466.
22. Larsen, P. (1955) in *Modern Methods of Plant Analysis,* eds. Paech, K. & Tracey, M. V. (Springer, Berlin), Vol. 3, pp. 565–625.
23. Gutknecht, J. & Walter, A. (1980) *J. Membr. Biol.* **56,** 65–72.
24. Cleland, R. E. (1976) *Plant Physiol.* **58,** 210–213.
25. Jacobs, M. & Ray, P. M. (1976) *Plant Physiol.* **58,** 203–209.
26. Roberts, J. K. M., Ray, P. M., Wade-Jardetzky, N. & Jardetzky, O. (1980) *Nature (London)* **283,** 870–872.